CONF-941144--104

Note: This is a preprint of a paper being submitted for publication. Contents of this paper should not be quoted nor referred to without permission of the author(s).

Submitted to the Materials Research Society 1994 fall meeting, Symposium A, *Beam-Solid Interactions for Materials Synthesis and Characterization*, ed. by D. E. Luzzi, M. Iwaki, T. F. Heinz, and D. C. Jacobson.

Fabrication and Modificcation of Metal Nanocluster Composites Using Ion and Laser Beams

R. F. Haglund, Jr., D. ~~O~~ H. Osborne, Jr., and R. H. Magruder, III
Vanderbilt University
Nashville, TN

C. W. White and R. A. Zuhr
Oak Ridge National Laboratory
Oak Ridge, TN

P. D. Townsend and D. E. Hole
University of Sussex
Brighton, United Kingdom

R. E. Leuchtner
University of New Hampshire
Durham, NH

DISCLAIMER

This report was prepared as an account of work sponsored by an agency of the United States Government. Neither the United States Government nor any agency thereof, nor any of their employees, makes any warranty, express or implied, or assumes any legal liability or responsibility for the accuracy, completeness, or usefulness of any information, apparatus, product, or process disclosed, or represents that its use would not infringe privately owned rights. Reference herein to any specific commercial product, process, or service by trade name, trademark, manufacturer, or otherwise does not necessarily constitute or imply its endorsement, recommendation, or favoring by the United States Government or any agency thereof. The views and opinions of authors expressed herein do not necessarily state or reflect those of the United States Government or any agency thereof.

"The submitted manuscript has been authored by a contractor of the U.S. Government under contract No. DE-AC05-84OR21400. Accordingly, the U.S. Government retains a nonexclusive, royalty-free license to publish or reproduce the published form of this contribution, or allow others to do so, for U.S. Government purposes."

Prepared by the
Oak Ridge National Laboratory
Oak Ridge, Tennessee 37831
managed by
MARTIN MARIETTA ENERGY SYSTEMS, INC.
for the
U.S. DEPARTMENT OF ENERGY
under contract DE-AC05-84OR21400

MASTER

December 1994

DISTRIBUTION OF THIS DOCUMENT IS UNLIMITED

GH

DISCLAIMER

Portions of this document may be illegible in electronic image products. Images are produced from the best available original document.

FABRICATION AND MODIFICATION OF METAL NANOCLUSTER COMPOSITES USING ION AND LASER BEAMS

R. F. HAGLUND, Jr.,* D. H. OSBORNE, Jr.,* R. H. MAGRUDER, III,** C. W. WHITE,‡ R. A. ZUHR,‡ P. D. TOWNSEND,‡‡ D. E. HOLE‡‡ and R. E. LEUCHTNER❖
*Department of Physics and Astronomy and **Department of Applied and Engineering Science, Vanderbilt University, Nashville, TN 37235. ‡Solid State Division, Oak Ridge National Laboratory, Oak Ridge, TN 37831; ‡‡School of Mathematical and Physical Sciences, University of Sussex, Brighton BN1 9QH, UK; and ❖Department of Physics and Astronomy, University of New Hampshire, Durham, NH 03824-3568

ABSTRACT

Metal nanocluster composites have attractive properties for applications in nonlinear optics. However, traditional fabrication techniques — using melt-glass substrates — are severely constrained by equilibrium thermodynamics and kinetics. This paper describes the fabrication of metal nanoclusters in both crystalline and glassy hosts by ion implantation and pulsed laser deposition. The size and size distribution of the metal nanoclusters can be modified by controlling substrate temperature during implantation, by subsequent thermal annealing, or by laser irradiation. We have characterized the optical response of the composites by absorption and third-order nonlinear-optical spectroscopies; electron and scanning-probe microscopies have been used to benchmark the physical characteristics of the composites. The outlook for controlling the structure and nonlinear optical response properties of these nanophase materials appears increasingly promising.

INTRODUCTION AND MOTIVATION

Suspensions of nanometer-size metallic particles have been used literally for millenia to color glasses for decorative purposes and to serve as building blocks for filters and other passive optical elements. The nonlinear optical response of metal nanocluster composites of this type have been studied extensively only within the last decade, however. Au nanoclusters in solution[1] and in ruby-gold glass,[2] and Ag nanoclusters in melt glass[3] are known to have picosecond nonlinear response times.[4] Cu:SiO_2 and Au:SiO_2 nanocomposites made by ion implantation exhibit picosecond nonlinear response times, with effective third-order susceptibilities several hundred times larger than those of colloidal melt glasses.[5] Metal species, substrate composition and size and size distribution of the metal nanoclusters all seem to play a role in the ultrafast electronic response to laser light signals. Thus, it seems likely that metal quantum-dot composites are intrinsically interesting and attractive as photonic materials.

If these materials are to become viable elements of photonic devices, two major problems must be confronted. One is fabricating metal quantum-dot composites cheaply and from materials which are compatible with future light sources and with electronic and superconducting materials used in hybrid electro-optic and magneto-optic devices; the other is controlling quantum-dot size and size distribution to satisfy specific optical and electronic-structure requirements. A number of synthetic techniques have now been shown to be effective in making metal quantum-dot composites, including ion implantation,[6,7] dual-target magnetron sputtering,[8] and pulsed laser deposition. Mean quantum-dot sizes and size distributions can be controlled to a limited extent by thermal annealing[9] and by varying ion-beam current density.[10]

In this paper, we describe how lasers and ion-beams can be used both to fabricate metal quantum-dot composites, and to use lasers in a post-processing step to modify the nonlinear optical response of nanocomposites comprising various metal species in a number of dielectric hosts, including both linear and nonlinear substrates. We describe the modification of the nonlinear optical response by laser irradiation and infer that the laser annealing is reducing the mean size of the metal quantum dots in these nanocomposites. Finally, we consider mechanisms which may be able to account for the apparent reduction in quantum-dot size manifested in the appearance of large nonlinear saturation effects following laser post-processing.

THE ROLE OF QUANTUM-DOT SIZE IN NONLINEAR OPTICAL RESPONSE

The local structure of a nanocomposite material is shown schematically in Figure 1. The metal quantum dots are assumed to be separated sufficiently that there are no interactions between dots. Under these conditions, the electrons in a metal quantum dot embedded in an insulating matrix can be treated as a system of n independent electrons confined to a spherical box, with an electronic structure consisting of distinct, though perhaps overlapping, energy levels.[11] Optical transitions in the quantum dots may be described using density matrix formalism for a two-level system in contact with a reservoir of unexcited material. Despite the simplicity of this model, the results it produces give zeroth-order clues to the materials parameters which can reasonably be measured via third-order non-linear optics.

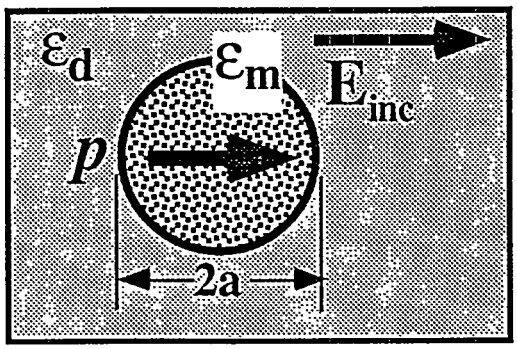

Figure 1. Schematic diagram of a metal quantum dot embedded in a dielectric.

Three distinct optical transitions are allowed in metal quantum dots: (1) hot-electron transitions, in which electrons near the Fermi level absorb energy from incident light; (2) interband transitions between the localized d orbitals of the metal valence bands and empty conduction band states; and (3) intraband transitions from filled conduction-band states near the Fermi edge to empty states higher in the conduction band. The latter two are shown schematically in Figure 2.

The nonlinear optical response of electrons in a metal quantum-dot material is most strongly affected by two confinement effects: one a classical effect due to electric-field enhancement, the other a quantum-mechanical effect due to the spatial constriction of the electronic wave functions. The classical confinement effect produces a local field enhancement associated with interband transitions; it is also the cause of the surface plasmon resonance. Interband effects can be greatly enhanced by embedding metal quantum dots in a nonlinear dielectric.[12]

The quantum confinement effect, on the other hand, is especially pronounced for the *intra*band transitions where both the initial and final states experience the confinement due to the shortened mean free path between electron collisions with the hard boundary separating metal and dielectric. The quantum-confined electronic susceptibility is proportional to the inverse cube of the dot radius, and rapidly increases in magnitude below particle diameters of approximately 10 nm, as we have demonstrated for Cu dots in fused silica.[13] This makes small average quantum-dot diameter especially desirable for enhanced third-order susceptibility — the nonlinear effect associated with nonlinear refraction and optical switching.

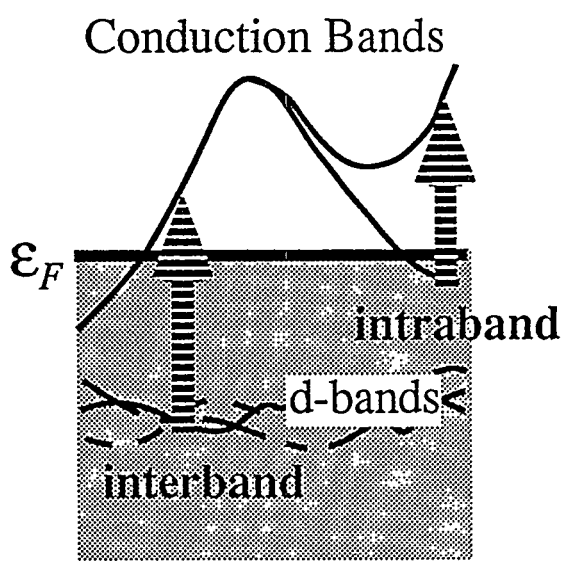

Figure 2. Schematic diagram of optical transitions in a noble-metal quantum dot.

Size effects have different origins in metal and semiconductor quantum dots. When the radii of unwanted excitonic states are larger than the particle size, the absorption spectrum (*i.e.*, electronic structure) consists of discrete lines broadened by lifetime and thermal (phonon) effects. The oscillator strengths associated with transitions between these discrete or quasi-discrete states are large compared to those for transitions between bulk bands. Nonlinear optical properties are enhanced, since one can saturate the lowest interband transition — for appropriately chosen particle size — with only one photon (one *e-h* pair) per nanoparticle.[14] Thus narrow size distribution is vital to optimum nonlinear optical performance of a semiconductor quantum-dot composites, but probably plays a less significant role in metal quantum-dot composites.

FABRICATION BY BEAM-ASSISTED DEPOSITION

We have explored two different kinds of beam-assisted deposition for fabricating metal quantum dot composites: ion implantation, and pulsed laser deposition, each of which has unique problems and capabilities.

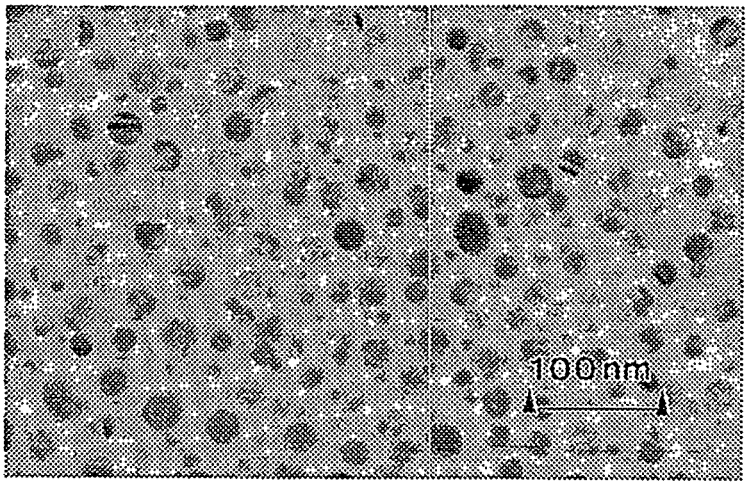

Figure 3. Plan view, transmission electron micrograph of a Cu:silica nanocomposite synthesized by ion implantation at a substrate temperature of 600° C.

One class of nanocomposites was prepared by implanting metal ions into synthetic silica, float glass and sapphire substrates at beam energies ranging from 60 to 3,500 keV. Nominal ion doses were in the range 0.1-15·10^{16} ions·cm^{-2}; with current densities varying from 0.7 to 7.5 μA·cm^{-2}. At these energies, the ion range (100-500 nm) is determined primarily by the nuclear stopping power of the substrate; the depth distribution of the particles is roughly Gaussian (in the case of Ag and Cu, sometimes bimodal), with a full-width at half maximum typically comparable to the mean ion range. The number of metal atoms in the implanted layer is of order 10^{20} cm^{-3}, so the nanocomposite has a large volume fraction of metal ions (~ 5%) compared to that attainable in conventional melt glass, but also exhibits substantial bond-breaking and defect formation. A micrograph of a Cu:SiO_2 nanocomposite is shown in Figure 3.

The concentration and depth profile of the implanted metal ions — but not their state of aggregation — were determined in the ion-implanted samples by Rutherford backscattering (RBS) of 2 MeV He^+ ions. In general, the RBS profiles show that the metal has a nominally Gaussian distribution about the mean depth of 100-400 nm. However, both Ag and Cu implants can, under some circumstances, develop a bimodal distribution. In these cases, the size distribution of the metal quantum dots may vary as a function of the depth in the nanocomposite layer.

Samples for nonlinear optical studies were also made by pulsed laser deposition.[15] The pulsed laser deposition technique (PLD) has been successfully used to prepare a great variety of multicomponent epitaxial thin films.[16] PLD offers significant advantages over other thin-film deposition techniques: epitaxial films are formed at relatively low substrate temperatures; PLD produces films that are often stoichiometric with respect to the target; high pressures of reactive ambients can be used; and no toxic or hard-to-prepare precursors are required. The technique is easy to implement and involves relatively few experimental "knobs" to adjust. Among the many diverse applications of PLD films are microelectronics,[17] acousto-optics,[18] sensors,[19,20] and biomaterials.[21]

Trilayer films of Pt clusters embedded in barium titanate were prepared under typical PLD processing conditions. The ablation laser was a KrF excimer device (20 ns, 248 nm), focused to fluences of about 3-4 J·cm^{-2} at the target surface, producing typical deposition rates of 0.01 nm metal per laser shot. The PLD chamber was pumped down to a base pressure of 1·10^{-7} torr and the substrate, ⟨100⟩-MgO, was heated in vacuum to 600° C. The first layer of about 0.5 μm of $BaTiO_3$ was deposited by ablating a BaO/TiO_2 pressed oxide pellet in 0.3 torr of O_2. The film was cooled to less than 200° C in 760 torr O_2, then the target was changed to one of the metals (Au, Ag, Pt, or Cu), the system pumped down to base pressure again and the substrate heated to 600° C. The metal was deposited in 0.050 torr of Ar, using anywhere from 100 to 1,000 laser shots. At these temperatures and pressures, the metal layer was composed of small aggregate islands that started at several nm in diameter and coalesced as the deposition continued.[22] The metal layer was cooled below 200° C in 760 torr of Ar to minimize oxide formation; then the target was changed back to $BaTiO_3$ and the second layer (~1 um in 10,000 laser shots) was deposited under the same conditions as the first.

PHYSICAL AND OPTICAL CHARACTERIZATION

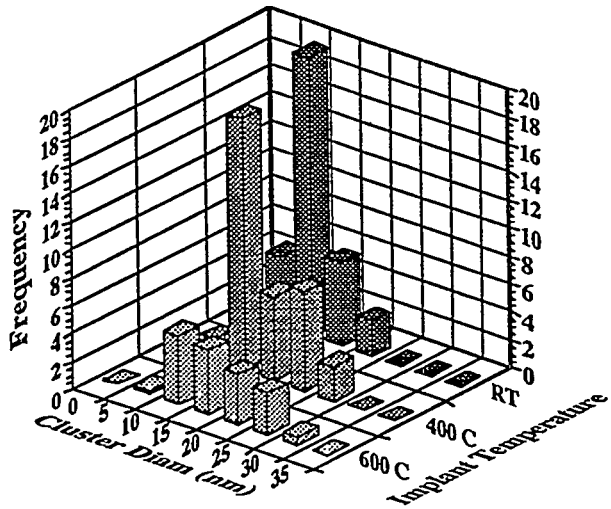

Figure 4. Histogram of the size distributions for Cu:silica nanocomposites synthesized by ion implantation at three different substrate temperatures.

The size distributions and geometrical structure of metal nanoclusters in selected composite materials were determined by transmission electron microscopy (TEM). Samples were examined in a 200-keV scanning transmission electron microscope, using bright field and dark field imaging, both normal to and at 45° to the plane of the sample, and selected-area electron diffraction (SAD) techniques. Samples implanted at the highest current density were stable in the TEM, while samples implanted at lower current densities required carbon coating to eliminate charging effects. Detailed TEM studies of Cu:silica nanocomposites have appeared elsewhere.[23]

The SAD patterns for metal nanoclusters in the silica substrate show a concentric ring pattern characteristic of electron diffraction from randomly oriented, mostly single-crystal metallic crystallites, superimposed on the diffuse diffracted intensity from the glass matrix. This is to be expected given that there is no preferred direction in the substrate materials; the nanoclusters grow in orientations determined by the most local silica structure. In Cu- and Ag-implanted silica, no evidence for any metallic compounds (*e.g.*, Cu-oxides) was observed.

Figure 3 shows a TEM micrograph of a Cu:silica nanocomposite prepared at 600° C. As the substrate temperature during implantation was decreased for the same dose rate and total dose, it was found that the mean cluster size decreased by 70%, the size distribution was broadened as shown in Figure 4.[24] A similar result was observed for $Cu:SiO_2$ nanocomposites prepared at the same substrate temperature but at decreasing dose rate and concomitant increase in the rate of local energy deposition.[23] The observed changes in size and size distribution were consistent with diffusion kinetics of the implanted copper with due regard for local energy deposition.

These changes in the measured size distribution are reflected in the optical absorption spectra. Figure 5 shows the optical absorption spectra for the three $Cu:SiO_2$ samples, the size distributions of which are displayed in Figure 4. It should be noticed that the sample with the sharpest optical absorption resonance is the one with the broadest size distribution and largest mean size; this confirms the point that the linear first-order) susceptibility decreases with decreasing cluster size. The third-order susceptibility, on the other hand, shows the opposite

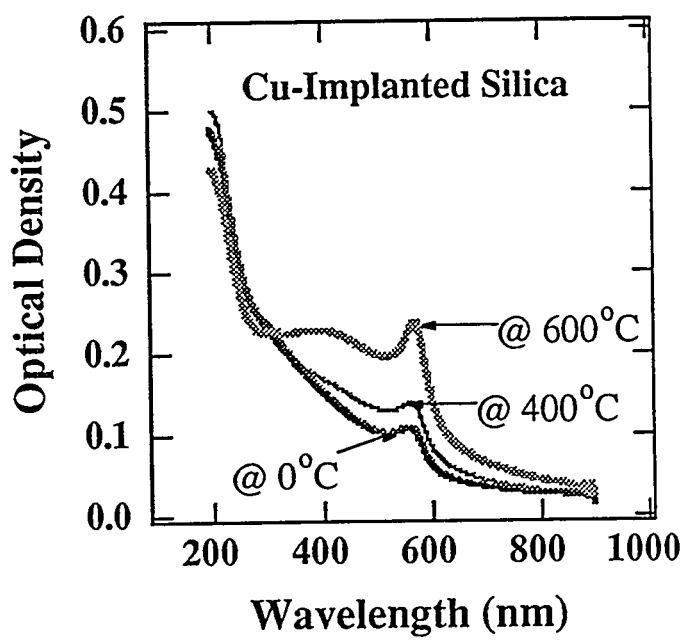

Figure 5. Absorption spectra for the three Cu-implanted silica samples shown at left. Note the growth of the surface-plasmon peak as the temperature increases.

behavior, at least for intraband optical transitions: the quantum confinement effect increases nonlinear optical response inversely as the cube of the nanocluster diameter.

The trilayer films synthesized by pulsed-laser deposition were analyzed by x-ray diffraction (XRD), scanning electron microscopy (SEM), atomic force microscopy (AFM), and uv-vis spectrophotmetry. Previous studies[22] of Pt deposited on MgO and $PbTiO_3$ indicate that, although island growth develops as the metal is being deposited, presumably due to poor wetting of the oxide surface, the small islands grow along the preferred orientation of the substrate. In Figure 6 are shown two XRD spectra: (a) of the first BaTiO3 layer and (b) the composite $BaTiO_3/Pt/BaTiO_3$ trilayer system. The tetragonal splitting is evident in the first $BaTiO_3$ layer for the {001} reflections; this layer gave a rocking curve width of about 0.2°, suggesting the highly oriented nature of the film. The tetragonal splitting of the second layer was not observed, indicating some degradation in quality of the final capping layer. A small peak near 39° in the composite film is likely ⟨111⟩ oriented Pt. The metal layers are typically too thin to observe with our diffractometer.

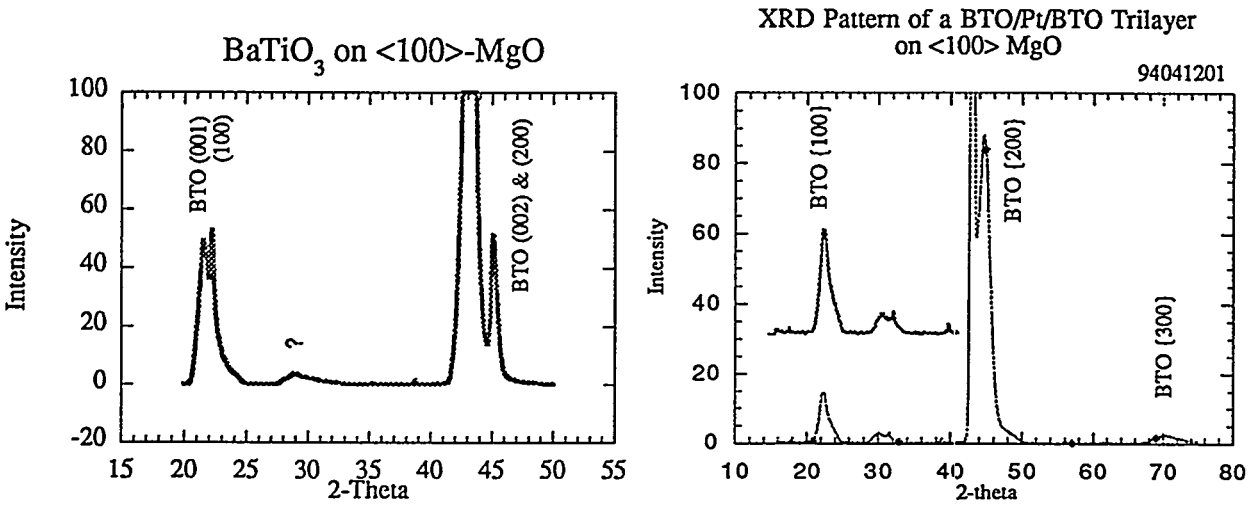

Figure 6. X-ray diffraction spectra for two samples grown by pulsed laser deposition: (left) barium titanate on magnesium oxide; (right) a trilayer barium-titanate/platinum/barium titanate film on magnesium oxide.

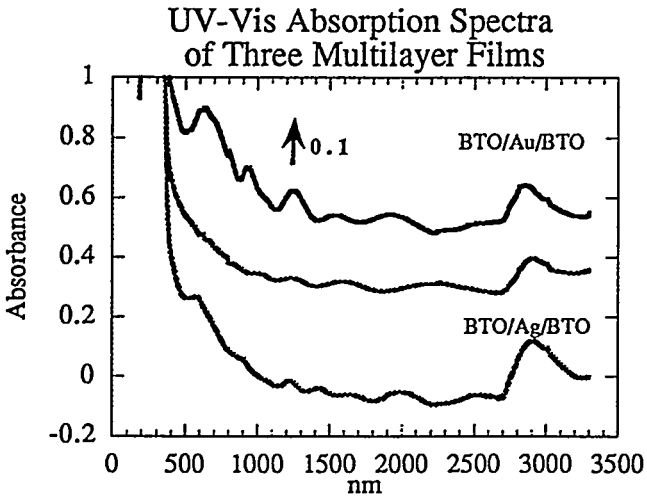

Figure 7. Ultraviolet-visible spectrum of films grown by pulsed-laser deposition.

Although *in-situ* analysis of the exact film thicknesses was not carried out, a fit to interference maxima based on the uv-vis spectra (300-3,000 nm), yielded film thicknesses that ranged from 1200 to 1800 nm. Several uv-vis absorption spectra are shown in Figure 7 for embedded Au and Ag nanoclusters, as well as a MgO blank, deposited under otherwise identical conditions but with no metal deposition. The absorption peaks near 570 nm (for Ag) and 620 nm (for Au) are likely due to the surface plasmon resonance, while the absorption feature at ~2900 nm is probably due to the $BaTiO_3$ matrix.

AFM studies on the surface topography of completed trilayers show a typical rms surface roughness of about 40-70 nm with a range of grain sizes (0.1-0.5 μm). Scanning electron microscopy confirmed some of the AFM results, although charging of the $BaTiO_3$ surface precluded significant detailed analysis (the nonlinear optical analysis would have been tainted if the samples

were conductively coated). AFM analysis of the size of the metal islands *prior* to the deposition of the final $BaTiO_3$ layer showed that approximately 250 laser shots produced islands of ~10 nm in diameter with a surface density in the range of $1\text{-}10 \cdot 10^{12}$ cm^{-2}.

LASER-INDUCED MODIFICATIONS OF NONLINEAR OPTICAL RESPONSE

In the first reported experiment[25] on laser effects on size distributions of metal quantum dots in nanocomposites, it was observed that ultraviolet laser annealing at peak intensities of order 10 $MW \cdot cm^{-2}$ led to a loss of Ag from the nanoclusters; RBS analysis showed that the silver was being "lost" into the interstitial regions of the implanted host material. In contrast, thermal annealing of Ag:glass produced a shift in the surface-plasmon resonance (absorption) spectrum consistent with a reduction in nanocluster size and no loss of Ag metal. Here we report on measurements of the *nonlinear* response in nanocomposites subjected to intense visible laser irradiation at 532 nm, with photon energies too low to induce electronic transitions in the composite materials.

Measurements of the nonlinear absorption coefficient, and of the magnitude and sign of the nonlinear index of refraction, were made by means of the Z-scan technique,[26] a sensitive single-beam technique based on the transformation of phase distortion to amplitude distortion by beam propagation through a nonlinear medium. In the Z-scan, a Gaussian laser beam is tightly focused

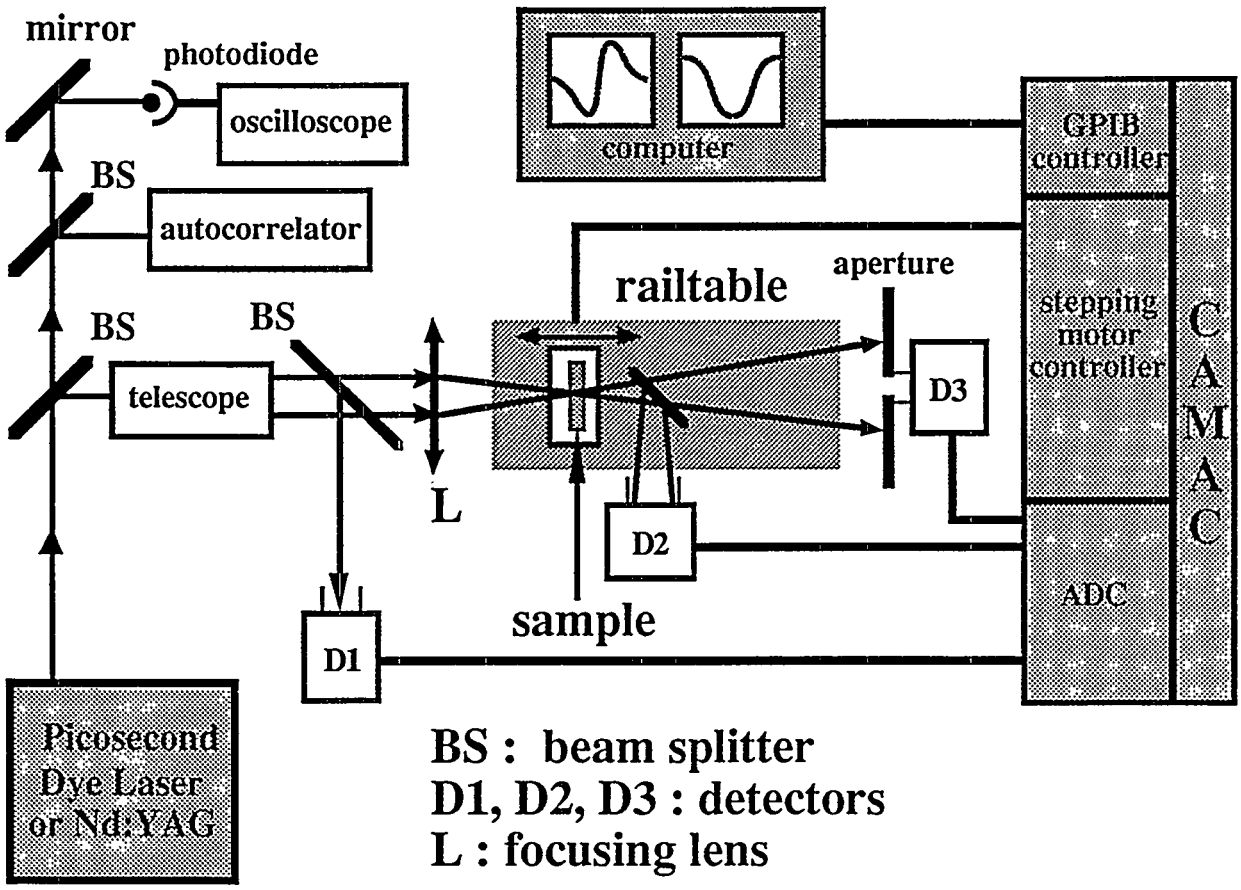

Figure 8. Schematic of experimental apparatus for simultaneous measurements of near-field and far-field beam transmission as a function of intensity (Z-scan).

onto a nonlinear medium which has a thickness small compared to the Rayleigh range. The sample can be moved parallel to the beam axis through the focal point of the lens to vary the intensity on the irradiated area of the sample. The transmission of the sample through a variable aperture on the optical axis of the beam in the far field, and to a detector collecting the whole beam in the near

field, was measured as a function of the sample position z, with respect to the focal plane. The plot of the power transmitted through the aperture versus z can be interpreted to yield the sign and the magnitude of n_2. The Z-scan is somewhat easier to implement than the conventional four-wave-mixing experiment, and, because it is a single-beam technique, makes it possible to make rapid comparisons among different classes of material. However, the Z-scan also requires careful optical alignment and strict attention to the mixing of thermal and electronic nonlinearities when working with a mode-locked laser system. In our Z-scan measurements, we used a mode-locked, cavity-dumped tunable dye laser with a pulse duration of 6 ps (as measured by standard auto-correlation techniques) and a pulse repetition frequency of 3.8 MHz, and a mode-locked, frequency-doubled Nd:YAG laser with a pulse duration of approximately 100 ps and a pulse repetition frequency of 76 MHz. The diameter of the laser focal spot was measured to be 35-40 μm at the focal plane of the Z-scan lens. Figure 8 shows a diagram of the apparatus as currently implemented in our laboratory. The Z-scan spectra were acquired and analyzed using the program IGOR; nonlinear least-squares fitting routines were employed to extract the nonlinear susceptibility.

For a thin nanocluster layer embedded in a transparent dielectric and for a high-repetition-rate laser, the relative far-field transmitted power is given by[27]

$$P_{\mathrm{det}} = \left[\frac{1}{1+\beta I_0 L \cdot \frac{1-exp(-\alpha L)}{\alpha}} \right] \cdot \left[\frac{C_1}{(1+\zeta^2)^2} + \frac{C_2}{(1+\zeta^2)} - 1 \right]^{-1} \tag{1}$$

where

$$C_1 = \frac{2LP_{inc}}{\pi n_0^2 r_0^4}, \quad C_2 = \frac{LP_{inc}K_T}{\pi n_0^2 r_0^4}, \quad \zeta \equiv \frac{z}{z_0}, \quad z_0 = \frac{\pi r_0^2}{\lambda} \tag{2}$$

P_{inc} is the total power on the sample; $I_0 = P/(4\pi r_0^2)$ is the intensity at the focal plane, with r_0 the usual Gaussian beam radius; L is the sample thickness; K_T is a material-dependent, thermo-optic coefficient; and α and β are, respectively, the one- and two-photon absorption coefficients.

The electronic and thermal contributions to the nonlinear index of refraction, and the two-photon absorption coefficient, were extracted from the Z-scan data using Eq. (1). Critical to these analyses is the fact that the z-dependence of the electronic and thermal components of the transmitted intensity are different (see Eq. (1)), making it possible to extract a semi-quantitative indication of the relative contributions of thermal and electronic mechanisms to the nonlinear optical response of the composite.

Figure 9 shows the measurements of the nonlinear absorption and index of refraction in an Au:silica nanocomposite using the tunable 6-ps dye laser described earlier. Average laser output power varied from 100 mW to 200 mW in TEM_{00} mode. The pulse repetition frequency was 3.8 MHz; the pulse width was about 5.5 ps. Under our experimental conditions, one can calculate that the Rayleigh range z_0 will be related to the characteristic thermal and electronic peak-to-valley distances

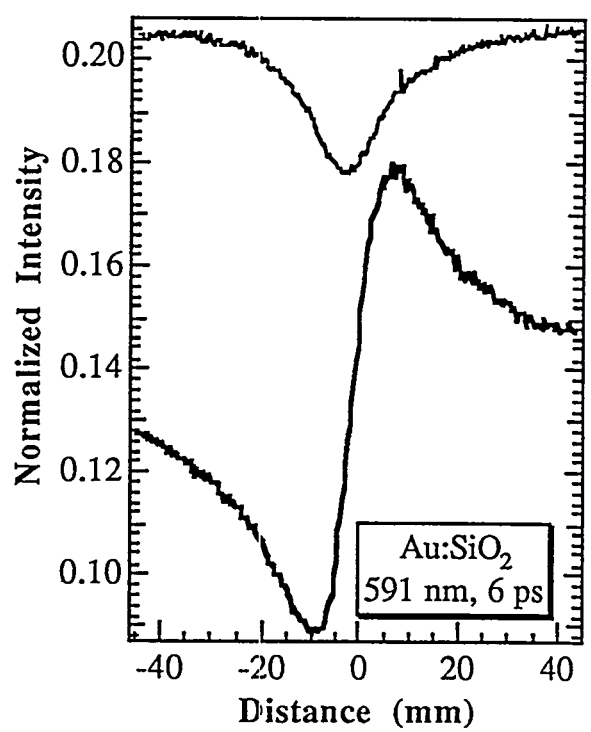

Figure 9. Near- and far-field Z-scan spectra of an Au:silica nanocomposite at 591 nm.

by $(2\sqrt{3}/3)z_0 = 10$ mm and $2z_0 = 17.3$ mm. The lower spectrum in Figure 9 shows a typical far-field Z-scan for this sample. The distance z between the valley and the peak of the z-scan spectrum is closer to $(2\sqrt{3}/3)z_0 = 10$ mm than to $2z_0 = 17.3$ mm. This fact indicates that even though both (fast) electronic and (slow) thermal effects contribute to the nonlinear refractive index, the thermal effects do not dominate the index nonlinearity for short laser pulses at a lower pulse repetition rate. Fitting the data for both the Nd:YAG and dye laser yields both the nonlinear index of refraction and two-photon absorption coefficients for this particular nanocomposite.

As the sample is transported through the focal plane of the fixed lens during the Z-scan, the laser intensity is also, of course, being varied. The peak intensity and the average power depend on the laser parameters. We used near-field and far-field measurements both to modify the materials and to measure the change achieved in their nonlinear response. In the following sequence of pictures, all of the scans are from metal-implanted float glass irradiated by the mode-locked pulse train from the frequency-doubled Nd:YAG laser. The peak intensity in the focal plane is approximately 10 $MW \cdot cm^{-2}$; it decreases quadratically with distance by roughly two orders of magnitude 10 mm on either side of the focal plane ($z = 0$) on the Z-scan translation stage.

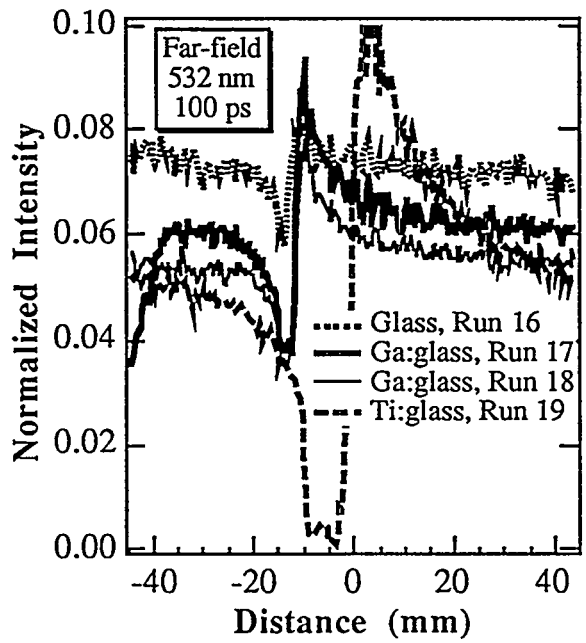

Figure 10. Far-field Z-scan spectra of float glass and of the same glass implanted with Ga and Ti.

In Figure 10, we see the far-field Z-scan spectra of a float glass substrate and of Ga:glass and Ti:glass nanocomposites. The dashed spectrum of the float glass substrate shows a small nonlinearity, probably due to the small amount of tin which diffuses into the top ten micrometers or so of the glass during the melt process. The two Ga:glass spectra were taken on successive runs a few minutes apart; the far-field spectrum itself is displaced from the zero of the scale by changing the "home" position of the stepping motor, in order to clearly display the differences between Ga:glass and Ti:glass materials. In the first run, the transmitted intensity increases immediately as the laser beam strikes the target. This is almost certainly due to the establishment of local thermal equilibrium and some vaporization; Ga is a liquid at room temperature when free, and it probably vaporizes easily under the intense laser irradiation. The next trace shows no sign of the incubation effect, and an only slightly diminished nonlinear refraction. The Ti:glass composite, on the other hand, shows a behavior much more like the typical response of a thermal refractive nonlinearity with a positive sign, with a steeper rise from peak to valley and a substantially larger overall index of refraction (proportional to the ratio of peak-to-valley amplitude). Previous Z-scan and optical absorption measurements in Ti:silica showed no sign of clustering, but did give evidence of strong thermal nonlinear refraction.

All of this suggests an extremely complex response to the laser annealing process which may involve not only thermal effects but relaxation effects over surprisingly long time scales. In an effort to unravel these complex effects, we studied the behavior of Ag:glass composites under varying conditions, using the whole-beam ("near-field") Z-scan both to vary the intensity of the annealing laser beam and, simultaneously, to measure the changes in the nonlinear saturation induced by the beam.

In the first experiment, the results of which are shown in Figure 11, the intensity of the laser irradiating the composite was varied an hundred-fold by removing or adding neutral-density filters in the laser beam prior to the focusing lens (L in Figure 8) until an effect was seen in the Z-scan

spectrum. The effect in this case was to produce a peak, instead of a dip, in the near-field transmission as the sample was scanned through maximum intensity near the focal plane. This is indicative of nonlinear saturation processes, rather than nonlinear absorption processes as exemplified in the upper spectrum of Figure 9. The wavelength of the laser used for these experiments — 532 nm — is far away from the interband transitions for the Ag nanoclusters, and, given the relatively long pulse duration (100 ps), we assume that we are primarily causing nonlinear responses by photothermal mechanisms. No effect was observed for a peak intensity of 1 MW·cm^{-2} (flat trace at the bottom of Figure 10). However, when the peak laser intensity was increased a factor of 10, we observed a nonlinear saturation that persists even when the beam intensity was subsequently lowered to 100 kW·cm^{-2}. Since the third-order susceptibility vanishes identically in bulk metal and hence must decrease with increasing nanocluster size, we infer that the effect of the laser beam is to reduce the mean cluster size. This conclusion agrees with that drawn from linear optical absorption measurements on KrF-laser-irradiated Ag:glass nanocomposites in Ref 25; however, the Z-scan measurement has the distinct advantage that it does not rely on the *absence* of an effect (*i.e.*, the lack of a shift in the surface-plasmon resonance) to support the hypothesis of a change in nanocluster size.

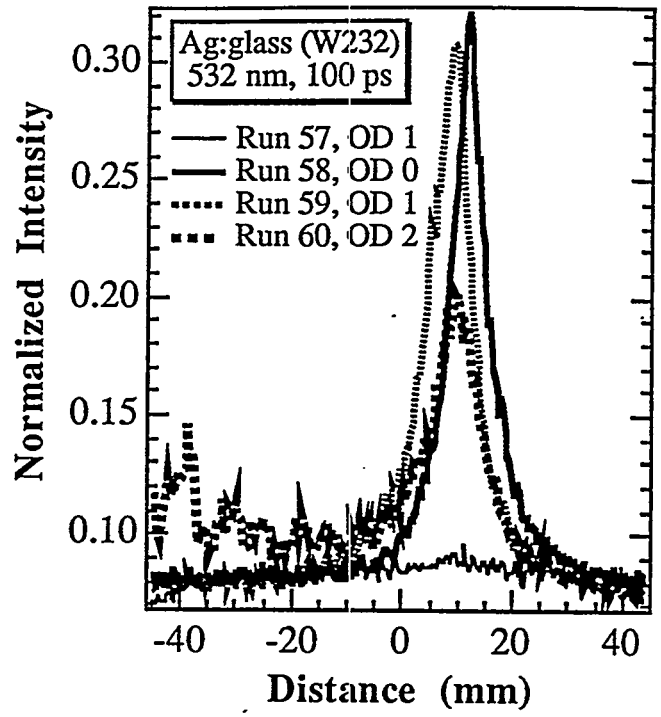

Figure 11. Near-field Z-scan spectra of Ag:glass nanocomposite starting from a pristine spot, using various attenuators. The four Z-scans are all normalized to the same intensity.

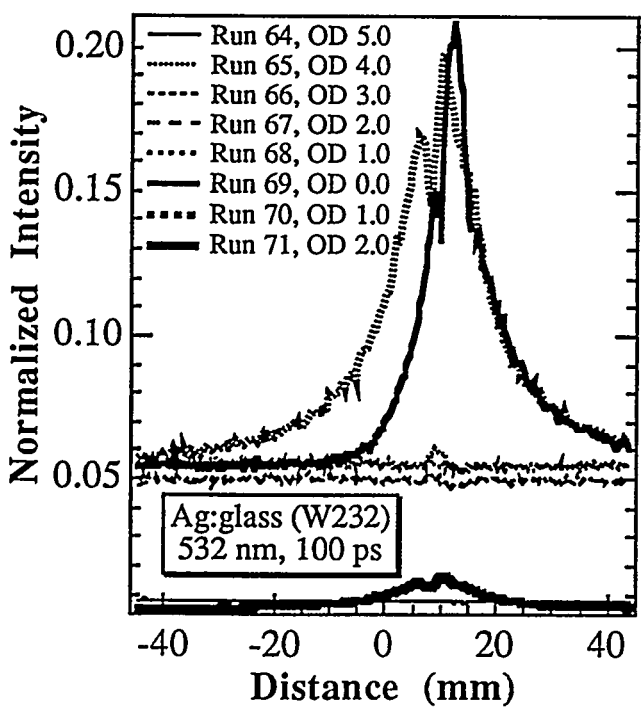

Figure 12. Near-field Z-scan of an Ag:float-glass nanocomposite showing the cumulative effect of gradually raising laser intensity over five decades.

We attempted to find the threshold for the irreversible change in the Ag:glass nanocomposite by starting at extremely low laser intensities, always scanning through the same spot on the sample. The results are shown in Figure 12. The lowest intensity — obtained by using a stack of neutral-density filters with an optical density of 5 (OD 5) — was about 0.1 kW·cm^{-2}. As shown in Figure 12, no nonlinear response was observed at all until the filter strength was reduced to OD 3 (10 kW·cm^{-2}), at which point there is the suggestion of a little ripple in the near-field Z-scan spectrum. However, once again there is no sign of the irreversible change in nonlinear optical re-

sponse until all the attenuators are removed from the beam and it reaches a peak intensity near the threshold value of 10 MW·cm^{-2}. The nonlinear absorption persists as low as 0.01 times full intensity once the irreversible change has taken place at the high laser power (OD 0). Moreover, there is a horizontal shift in the position of the peak nonlinear saturation from 4 mm to the right of the Z-scan focal plane to about 2 mm to the right. This indicates that the modification of the nonlinear response was taking place during the Z-scan and was continually modified during the measurement at higher powers, possibly with diffusive motion of the clusters closer to the focal plane of the lens at $z = 0$.

Clearly, the laser post-processing has a dramatic effect on the nonlinear response, and it would be desirable to know whether long-term laser irradiation could affect the nonlinear optical response. We studied this effect by starting below the modification threshold, then continuing to irradiate after the first signs of an altered nonlinear response appeared, then measuring the nonlinear response again. Figure 13 shows that there is no nonlinear effect at low power (OD 2). Nonlinear saturation occurs at full power (OD 0), and the nonlinear response increases when a second Z-scan is performed. After five minutes of continuous irradiation by the laser, still at full power, there has been little change, indicating stabilization of the clusters in the implanted layer, as indicated by the third Z-scan. The "notch" in the final Z-scan spectrum, closer to the focal plane than the principal saturation peak, suggests that the clusters are moving back toward the focal plane, perhaps due to a laser-induced migration effect due to local heating by the laser beam.

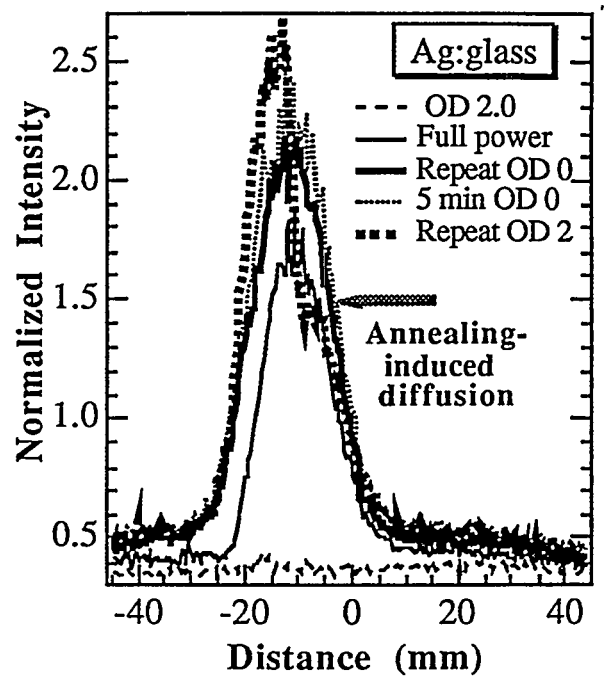

Figure 13. Near-field Z-scan spectra for the Ag:glass nanocomposite after repeated irradiation by the frequency-doubled Nd:YAG laser (532 nm).

MECHANISMS OF NANOCLUSTER MODIFICATION

The mechanism by which the metal quantum dots are altered by laser annealing is especially interesting and, at this point, somewhat mysterious. On one hand, there is evidence that the ultraviolet laser annealing produces a purely thermal effect governed by absorption and subsequent evaporation in the composite layer. It has already been proposed that laser annealing triggers the diffusion of Ag metal vaporized from clusters into the bulk of the material. There is RBS evidence of actual metal loss in some cases. Three groups have suggested, on the basis of experiments with ion-implanted glasses, that this might well be due to the Soret effect,[28] in which there is differential diffusion toward the surface, and possibly evaporation of implanted atoms from the surface, because of the much steeper thermal gradient in that direction. The Townsend group have proposed that KrF laser annealing of Ag:glass nanocomposites produces evaporation from clusters into the bulk of the substrate.[25]

However, there is also intriguing evidence that non-thermal mechanisms could produce preferential sizing effects, hinting at the possibility for control of cluster size distributions by wavelength-selective "laser trimming." In experiments at the universities of Heidelberg and Kassel,[29] thermal-velocity alkali-metal atoms striking lithium fluoride surfaces in ultrahigh vacuum aggregated at defect sites to form clusters. When irradiated with light from wavelength-selectable krypton and argon ion lasers at irradiance levels as small as 50 μW·cm^{-2}, metal atoms were efficiently desorbed from the cluster surfaces. Localization of the laser energy required for nonthermal

desorption is guaranteed by the small size of the clusters: the absorbed energy is communicated electronically to desorbing atoms faster than it can "leak away" into lattice degrees of freedom. Two different size-related effects were observed: Tuning the laser light to the surface plasmon resonance frequency produced the most efficient desorption. However, tuning away from the plasmon frequency also changed the "size resonance" of the clusters; prolonged irradiation reduced the mean cluster size and narrowed the size distribution function as well. For nanoclusters embedded in a bulk dielectric, the confinement of the laser energy is even stronger and should, in principle, also be effective in leading to non-thermal vaporization.

The Kassel group proposed a model which describes the desorption rate of this resonant desorption process for particles of radius R, assuming that the size distribution is approximately Gaussian with the centroid at a radius R_λ characteristic of the laser wavelength. The model yields a rate equation for the number of desorbed or evaporated atoms N per unit time:

$$\frac{dN}{dt} = \sigma_0 \cdot I_{laser} \cdot Q f(R) \cdot R \exp\left\{ -\frac{(R-R_\lambda)^2}{2\beta^2} \right\} \cdot \Delta R \qquad (3)$$

where σ_0 is the absorption cross section for a cluster radius $R = R_\lambda$, I_{laser} is the laser intensity, N_c is the number of clusters within the illumination volume of the laser beam, Q is the quantum efficiency of the process, and β the width of the absorption profile.

We believe that similar effects may occur for metal nanoclusters in the bulk, producing an evaporative reduction in mean cluster size and perhaps changes in the size distribution. There is a free-volume fraction amounting to some 2.5% in fused silica networks compared with crystalline quartz; atoms evaporated from clusters thus have some "room" within the network. In the interior of ion-implanted solids, atoms ejected from cluster surfaces due to the excitation of the surface plasmon resonance will come to rest, perhaps as interstitials or, more likely, bonding to clusters at the small-radius tail of the cluster size distribution resonant with the laser wavelength. In this way, the cluster size distribution should be further narrowed without globally disturbing the thermal equilibrium of the implant or the glass substrate.

CONCLUSIONS

Our preliminary results confirm that it is possible to fabricate metal quantum-dot composites by both ion- and laser-beam deposition techniques. Varying ion-implantation parameters during synthesis of nanocluster composites modifies the size and the size distribution of metal quantum dots in relatively predictable and understandable ways. While experiments in waveguides have yet to be done, it seems likely that synthesis by pulsed-laser deposition is likely to be effective in making usable waveguides, since it is a deposition technique with, in principle, atomic-layer control. The nanocomposites created by both techniques show interesting nonlinear optical responses. Laser irradiation with both pulsed ultraviolet and mode-locked Nd:YAG can alter the nonlinear response of the composite by changing the size and/or size distribution of the metal nanoclusters. This provides an important new technique for controlling the size-dependent nonlinear optical response of the metal quantum-dot composites without damaging the host matrix. This must be tested by studies correlating nonlinear optical response with high-resolution microscopy of the nanophase composites.

ACKNOWLEDGEMENTS

Research at Vanderbilt is supported by the Army Research Office (contract DAAH04-93-G-0123), while experiments at Sussex are supported by a grant from the Science and Engineering Research Council of the UK. Collaborative studies between Vanderbilt and Sussex are supported by the North Atlantic Treaty Organization, Office of Scientific Affairs. Oak Ridge National Laboratory is partially supported by the Division of Materials Science, U. S. Department of Energy, under contract DE-AC05-84OR21400 with Martin-Marietta Energy Systems.

REFERENCES

1. M. J. Bloemer, J. W. Haus and P. R. Ashley, J. Opt. Soc. Am. B **7**, 790 (1990).
2. F. Hache, D. Ricard, C. Flytzanis and U. Kreibig, Appl. Phys. A **47**, 347 (1988).
3. J. W. Haus, N. Kalyaniwalla, R. Inguva, M. Bloemer and C. M. Bowden, J. Opt. Soc. Am. B **6**, 797 (1989).
4. C. Flytzanis, F.Hache, M.C. Klein, D. Ricard and Ph. Roussignol, Prog. Opt. **29**, E. Wolf ed., North Holland, Amsterdam (1991).
5. R. H. Magruder, III, R. F. Haglund, Jr., Li Yang, C. W. White, Lina Yang, R. Dorsinville and R. R. Alfano, Appl. Phys. Lett. **62**, 1730 (1993).
6. G. W. Arnold and J.A. Borders, J. Appl. Phys. 48, 1488 (1977)
7. R. F. Haglund, Jr., L. Yang, R. H. Magruder, III, J. E. Wittig, K. Becker and R. A. Zuhr, Opt. Lett. **18**, 373 (1993).
8. See, for example,A. Gavrin and C. L. Chien, J. Appl. Phys. **67**, 938 (1990).
9. C.R. Bamford, Colour Generation and Control in Glass, Glass Science and Technology, Vol. II (Amsterdam: Elsevier, 1977).
10. R. H. Magruder, III, R. F. Haglund, Jr., Li Yang and R. A. Zuhr, J. Appl. Phys. **76**, 781 (1994)
11. Li Yang, D. H. Osborne, R. F. Haglund, Jr., R. H. Magruder, C. W. White, R. A. Zuhr and H. Hosono, Appl. Phys. A, to be published.
12. A. E. Neeves and M. H. Birnboim, J. Opt. Soc. Am. B **6**, 787 (1989).
13. Li Yang, K. Becker, F. M. Smith, R. H. Magruder, III, R. F. Haglund, Jr., Lina Yang, R. Dorsinville, R. R. Alfano and R. A. Zuhr, J. Opt. Soc. Am. B **11**, 457 (1994).
14. R. Jain and R. C. Lind, J. Opt. Soc. Am. **73**, 647 (1983).
15. R. E. Leuchtner and R. F. Haglund, Jr., MRS Fall Meeting 1994, Paper Za7.4.
16. J. Cheung and H. Sankur, CRC Crit. Rev. Solid State Mater. Sci. **15**, 63 (1988). See also K. Saenger, Chap 20, in *Pulsed Laser Deposition*, D.B. Chrisey and G. Hubler, eds.(New York: John Wiley and Sons, 1994).
17. J.M. Pond, K.R. Carroll, J.S. Horwitz, D.B. Chrisey, M.S. Osofsky, and V.C. Cestone, Appl. Phys. Lett. **59**, 3033 (1991).
18. W. Jo, G-C. Yi, T.W. Noh, D-K Ko, Y.S. Cho, and S-I. Kwun, Appl. Phys. Lett. **61**, 1516 (1992). Y. Shibata, K. Kaya, K. Akashi, Appl. Phys. Lett. **61**, 1000-2 (1992).
19. M. Sayer, C.V.R.V. Kumar, D. Barrow, L. Zou and D.T. Amm, *in Ferroelectric Thin Films II* , eds. A. I. Kingon, E. R. Myers and B. Tuttle, Mater. Res. Soc. Symp. Proc. **243**, 39 (1992.
20. D. L. Polla, W. P. Robbins, T. Tamagawa and C. Ye, in Smart Materials Fabrication and Materials for Micro-Electro-Mechanical Systems, eds. A. P. Jardine, G. C. Johnson, A. Crowson and M. Allen, Mater. Res. Soc. Symp. Proc. **276**, 3 (1992).
21. C. M. Cotell, D.B. Chrisey, K.S. Grabowski, J.A. Sprague, and C.R. Gossett, J. Appl. Biomaterials **3**, 87 (1992). C.M. Cotell, Appl. Surf. Sci., in press .
22. R.E. Leuchtner, D.B. Chrisey, J.S. Horwitz, and K.S. Grabowski, Surface and Coatings Tech. **51**, 476 (1992).
23. R. H. Magruder, III, R. F. Haglund, Jr., Li Yang, J. E. Wittig and R. A. Zuhr, J. Appl. Phys. **76**, 708 (1994).
24. R.H. Magruder,III, D.L. Kinser, J.E. Wittig and R.A. Zuhr, Properties and Characteristics of Optical Glass III, Proc. SPIE **1761**, 180 (1992).
25. R. A. Wood, P. D. Townsend, N. D. Skelland, D. E. Hole, J. Barton and C. N. Alfonso, J. Appl. Phys. **74**, 5754 (1993).
26. M. Sheik-Bahae, A. A. Said, T. Wei, D. J. Hagan and E. W. VanStryland, IEEE J. Quant. Elect. **26**, 760 (1990).
27. K. Becker, L. Yang and R. F. Haglund, Jr., to be submitted to J. Opt. Soc. Am. B, 1995.
28. T. Shimizu, N. Itoh and N. Matsunami, J. Appl. Phys. **64**, 3663 (1988). A. Miotello and R. Kelly, Nucl. Instrum. Meth. Phys. Res. B **65**, 217 (1992). S. Y. Park, Ph.D. Thesis, Vanderbilt University, unpublished (1994).
29. W. Hoheisel, K. Jungmann, M. Vollmer, R. Weidenauer and F. Träger, Phys. Rev. Lett., **60**, 1649 (1988). M. Vollmer, R. Weidenauer, W. Hoheisel, U. Schulte and F. Träger, Phys. Rev. B **40**, 12 509 (1990).